



A new symmetrized solution for phase retrieval using the transport of intensity equation

V.V. Volkov^{a,*}, Y. Zhu^a, M. De Graef^b

^aDepartment of Materials Science, Brookhaven National Laboratory, Upton, NY 11973-5000, USA

^bDepartment of Materials Science and Engineering, Carnegie Mellon University, Pittsburgh, PA 15213-3890, USA

Received 30 November 2001; revised 8 January 2002; accepted 17 January 2002

Abstract

We propose a novel symmetrization method for solving the transport of intensity equation (TIE) using fast Fourier transforms for situations where the input images may or may not exhibit spatial periodicity. The method is derived from the analysis of intensity conservation law and the internal symmetry of the TIE, and is illustrated for both a computational and an experimental data set. © 2002 Elsevier Science Ltd. All rights reserved.

PACS: 42.30.Rx; 68.37.Lp; 75.60.Ch

Keywords: Phase retrieval; Transport of intensity equation; Lorentz microscopy

1. Introduction

The problem of phase retrieval from intensity measurements plays a key role in many fields of physics, such as optics, electron- and X-ray microscopy, diffraction, and NMR-tomography. In transmission electron microscopy, knowledge of both phase and amplitude enables direct mapping of the electrostatic and magnetostatic potentials of thin foil. In optics, holography, introduced originally by Gabor (1948), provides one approach to the problem of phase recovery. This technique is based on the analysis of experimental interferograms and is technically demanding. Teague (1982, 1983) suggested another essentially non-interferometric approach when he demonstrated that the phase of wave can be recovered from intensity measurements $I(x, y)$ by properly solving the transport of intensity equation (TIE), derived from the free space Helmholtz wave equation in the paraxial wave approximation. The TIE formalism is not restricted to coherent waves and works well for partially coherent beams, which makes phase reconstruction accessible to wide range of light- and electron-beam based experiments.

In the paraxial approximation, the propagation of monochromatic wave can be described in the coordinate system (\mathbf{r}_\perp, z) , where z denotes coordinate along the optical axis,

and \mathbf{r}_\perp is the position within plane normal to the optical axis. Taking the imaginary part of the paraxial wave equation (Gureyev and Nugent, 1996; Paganin and Nugent, 1998)

$$\left(\nabla_\perp^2 + 2ik\partial/\partial z\right) \cdot \sqrt{I(\mathbf{r}_\perp, z)} \exp[i\phi(\mathbf{r}_\perp, z)] = 0 \quad (1)$$

yields the TIE derived by Teague (1983) as

$$\nabla_\perp \cdot [I(\mathbf{r}_\perp, z) \nabla_\perp \phi(\mathbf{r}_\perp, z)] = -k \cdot \frac{\partial I(\mathbf{r}_\perp, z)}{\partial z} \quad (2)$$

where $k = 2\pi/\lambda$ is the radiation wavenumber, and $\phi(\mathbf{r}_\perp, z)$, the phase to be retrieved. The terms $I(\mathbf{r}_\perp, z)$ and $\partial_z I(\mathbf{r}_\perp, z)$ are the irradiance and its longitudinal derivative. The ∇_\perp differential operator operates only in the plane normal to the propagation direction. The TIE relates the forward propagation of the beam intensity to the lateral variations of the beam phase. The TIE is second-order elliptical differential equation and can be reduced further to the inhomogeneous Poisson equation by the introduction of an auxiliary function ψ (Teague, 1983), defined by (dropping the argument (\mathbf{r}_\perp, z) from here on):

$$\nabla_\perp^2 \psi = I \nabla_\perp \phi \quad (3)$$

This assumption means that vector $\mathbf{S} = I \nabla_\perp \phi$ will be further treated as vector field of some scalar potential ψ . Paganin and Nugent (1998) suggested to associate it with Poynting vector $\mathbf{S}(\mathbf{r}_\perp, z)$. The TIE (2) then reduces to Poisson equation

$$\nabla_\perp^2 \psi = -k \cdot \partial_z I \quad (4)$$

* Corresponding author. Tel.: +1-631-344-7355; fax: +1-631-344-4071.
E-mail address: volkov@bnl.gov (V.V. Volkov).

Implementing the TIE formalism in practice has been difficult. Several different solution methods for Eq. (2) have been suggested (Teague, 1983; Roddier, 1990; Gureyev and Nugent, 1996; Paganin and Nugent, 1998). However, only in special cases are the available algorithms of phase reconstruction sufficiently fast for reasonably sized images. Some algorithms only work well when zero image intensity is assumed outside the image area (Gureyev and Nugent, 1996), which may not reflect all real experimental situations, or will require the use of special apertures. Paganin and Nugent (1998) proposed an alternative definition of phase via the Poynting theorem and showed that TIE can be used with some limitations for general case, including electromagnetic fields. With assumption (3), a formal solution to TIE (2) is given by (Paganin and Nugent, 1998)

$$\phi(\mathbf{r}_\perp, z) = -k\nabla_\perp^{-2} \cdot \left\{ \nabla_\perp \left[\frac{\nabla_\perp \nabla_\perp^{-2} \partial_z I}{I} \right] \right\}, \quad I \neq 0 \quad (5)$$

where ∇_\perp^{-2} is the inverse Laplacian operator calculated by whatever appropriate method. The intensity I is assumed to be strictly positive. This solution will be sensitive to boundary constraints.

2. Theory

2.1. Fourier transform

It has been shown (Gureyev and Nugent, 1996; De Graef, 2001) that serious mathematical problems in solving the TIE with finite-elements methods can be bypassed by computing the inverse Laplacian ∇_\perp^{-2} via fast Fourier transforms (FFT):

$$\nabla_\perp^{-2} u(x, y) = F^{-1} \left[\frac{F[u(x, y)]}{|\mathbf{q}_\perp|^2} \right], \quad \mathbf{q}_\perp \neq 0 \quad (6)$$

The symbols F and F^{-1} represent here forward and inverse Fourier transforms, and the vector \mathbf{q}_\perp is the frequency vector normal to the propagation direction. However, any use of computer involves sampling data and hence periodic continuation in reciprocal space, and hence approximation of input images with Fourier series. This implies spatial periodicity of the input images, which is not generally valid for an experimental data set. Therefore, the question whether the FFT approach to the TIE phase problem is correct and unique in terms of the Dirichlet–Neumann boundary problem remains unanswered. Note that the existence of unique solution up to an arbitrary additive constant for the TIE problem was proven only for special case (Gureyev and Nugent, 1996), in particular, assuming zero intensity outside the image area, which is equivalent to recording an image through an opaque aperture.

2.2. Boundary conditions and energy conservation law

In the present paper, we provide the symmetry analysis to

the TIE. We prove that under the new Neumann boundary condition valid for a wide range of objects, specified below and derived from an intensity conservation law, the phase solution of the TIE obtained by FFT methods is correct and unique up to a constant. We propose also simple symmetrization rule for phase reconstruction that is free from edge-spoiling/aliasing effects in the entire area of an experimental image. This approach is especially important for correctly mapping magnetic induction in magnetic materials.

We start with analysis of the intensity conservation law, which is assumed to be valid for the TIE (Teague, 1982; Gureyev and Nugent, 1996):

$$\partial_z \iint_D I(\mathbf{r}_\perp, z) dx dy = 0 \quad (7)$$

This equation expresses that the total irradiance $I(\mathbf{r}_\perp, z)$ in planar image area $D(x, y)$ transverse to the z -direction of wave propagation is conserved when recorded at $z = z_0$ and $z = z_0 + \Delta z$. We integrate both sides of the TIE expression given by Eqs. (2)–(4) over the area D :

$$\iint_D \nabla_\perp^2 \psi(\mathbf{r}_\perp, z) dx dy = -k \partial_z \iint_D I(\mathbf{r}_\perp, z) dx dy \quad (8)$$

It is clear that the surface integral of $\nabla_\perp^2 \psi$ in Eq. (8) over the area D must vanish because of assumption (7). We also take advantage of the mathematical identity

$$\iint_D \nabla_\perp^2 u(x, y) dx dy = \oint_L [\mathbf{n} \cdot \nabla_\perp u] ds = \oint_L \frac{\partial u}{\partial \mathbf{n}} ds \quad (9)$$

which can be derived from Green's formula (Piskunov, 1965); here \mathbf{n} is the outward unit normal to the contour $L = \partial D$ of the domain D . Using this identity, Eq. (8) can be written as

$$-k \partial_z \iint_D I(\mathbf{r}_\perp, z) dx dy = \oint_L \frac{\partial \psi}{\partial \mathbf{n}} ds \quad (10)$$

It is just an expression of energy conservation law, which should replace Eq. (7) in more general case. Let us now analyze the conditions under which the right-hand side of Eq. (10) will vanish. By taking Eqs. (7)–(9) into account and the identity $\partial \psi / \partial \mathbf{n} = I \partial \phi / \partial \mathbf{n}$ from Eq. (3), we get

$$\oint_L \frac{\partial \psi}{\partial \mathbf{n}} ds = \oint_L I [\mathbf{n} \cdot \nabla_\perp \phi] ds = \oint_L I \frac{\partial \phi}{\partial \mathbf{n}} ds = 0 \quad (11)$$

Eq. (11) expresses that the function ψ does not 'leak' through the boundary L of the domain D , if Eq. (7) holds valid, and represents new 'natural' integral boundary condition for the solution of the TIE (2). With definition of $I \nabla_\perp \phi = \mathbf{S}(\mathbf{r}_\perp, z)$ as the Poynting vector or force vector field Eqs. (11) and (12) can be rewritten as

$$-k \partial_z \iint_D I(\mathbf{r}_\perp, z) dx dy = \oint_L \mathbf{n} \cdot \mathbf{S} ds = 0 \quad (12)$$

which states that intensity conservation law (7) will be valid

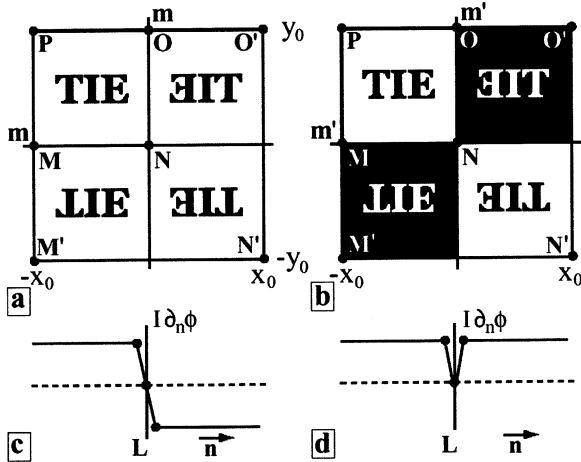


Fig. 1. Even (a) and odd (b) symmetric extensions of the original image MNOP satisfying the internal TIE symmetry and the Neumann boundary condition. Images (c) and (d) show the behavior of the function $I \cdot \partial \phi / \partial \mathbf{n}$ across the boundary L for the extended sampling data array.

only if the dissipation of energy flow \mathbf{S} through the contour L is negligibly small. In practice, it is possible to choose the image size D large enough comparing to object size, sufficient to null Eq. (12). Note that Gureyev and Nugent (1996) extensively studied special case of the boundary problem under the assumption of ‘zero intensity’ $I(L) = 0$ sufficient to satisfy Eqs. (11) and (12). They showed that the TIE solution in this case is unique up to a constant; however, the numerical approach to solve the TIE based on Zernike polynomials (Gureyev and Nugent, 1996) appears to be difficult in practice. In addition, it seems that such condition may not be consistent with the general assumption $I(D) \neq 0$ ($L \subseteq D$) used to solve the TIE problem via the formal solution of Eq. (5). Most of these complications can be bypassed when using Eqs. (11) and (12) under the new Neumann boundary condition

$$[\mathbf{n} \cdot \nabla_{\perp} \phi(L)] = \partial \phi(L) / \partial \mathbf{n} = 0 \tag{13}$$

and $I(L)$ finite function, which will satisfy the integral conditions (11) and (12) automatically. This is sufficient to get unique phase solution $\phi(D)$ of TIE problem described by Eqs. (2)–(4) and (13) apart from a constant term (Sneddon, 1957) equal, for instance, $2\pi n$ (n -integer) or any other constant. The alternative Neumann condition to Eq. (13) have been analyzed by Roddier (1990). However, Eq. (13) is a ‘stronger’ boundary condition than conditions (11) and (12). Hence, we have to define a class of images and objects, satisfying Eq. (13). We shall call it as imaging of objects wrapped with uniform phase support. Indeed, there exists a wide class of images with non-uniform illumination of objects, for which the phase behavior at circumference of image $[L - \delta, L]$ will tend to be a constant (i.e. $\nabla_{\perp} \phi \approx 0$ at $\delta \rightarrow 0$) and, hence, $\partial \phi(L) / \partial \mathbf{n} \approx 0$. As follows from Eq. (2), the intensity variation within the same boundary layer of width δ close to the image perimeter will also vanish, i.e.

$\partial I(L) / \partial z \approx 0$. Examples of this class of images will be given later.

2.3. Symmetrization rule

Now we investigate the numerical FFT-solutions (5) and (6) of TIE phase problems (2)–(4) with the new Neumann boundary condition (13) in the limit of $\delta \rightarrow 0$. This will reflect a loss of translational periodicity of the image and, hence, the correct use of numerical FFT will require some symmetrization of input images. It will be shown later that there exists an appropriate symmetrization of the original image intensity $I(\mathbf{r}_{\perp})$ distribution, automatically satisfying conditions (11)–(13).

We shall assume that the image area $D(x, y)$ is square with $N \times N$ sensing elements, such as the detector area provided by a CCD-camera. In this case, the contour integral in Eq. (11) splits into four line integrals taken along the x and y directions for the closed loop L , as shown by Eq. (14) and Fig. 1(a) and (b)

$$\oint_L I \frac{\partial \phi}{\partial \mathbf{n}} ds = \left[\int_O^P - \int_M^N \right] I \partial_y \phi dx + \left[\int_N^O - \int_P^M \right] I \partial_x \phi dy \tag{14}$$

It is clear that the contour integral in Eq. (14) will vanish under the trivial assumption $I(L) = 0$. Another less trivial and more useful boundary condition can be realized if symmetry criteria are applied both to Eq. (14) and the structure of the TIE (2). Notice that TIE has intrinsic symmetry, i.e. invariance under the transformation $I \rightarrow -I$. Taking into account boundary condition (13), the phase $\phi(x, y)$ can symmetrically be extended outside of original image D only as even function of the coordinates, regardless of the nature of $I(x, y)$ (odd or even). This means that we can extend the image $I(x, y)$ from the square area in which it was measured to square MNOP of double dimensions along both x and y (Fig. 1(a)). Since we wish to use the FFT algorithm to obtain the fast numerical solution of the equation, we must periodically extend the image so that both internal symmetries of the TIE and the boundary integral equation (11) are satisfied. It is easy to see that there are two possible symmetric extensions, shown in Fig. 1(a) and (b). The first extension use simple mirror planes \mathbf{m} along the bottom and right edge of the input image $M'N'O'P$ to obtain periodic continuation of the image. The second employs the $I \rightarrow -I$ invariance of the TIE and replaces the mirrored intensity by its negative in the lower left and upper right quadrants. If we group the integrals over the vertical edges in Eq. (14), we obtain

$$\int_{-y_0}^{y_0} I(x_0, y) \partial_x [\phi(x_0, y) \pm \phi(-x_0, y)] dy = 0 \tag{15}$$

for the even (top sign) and odd (bottom sign) symmetric extensions (and similar expressions for the integrals along the x -direction). The even extension implies that $I \cdot \partial_n \phi$ is an odd function across the integration contour, as shown in

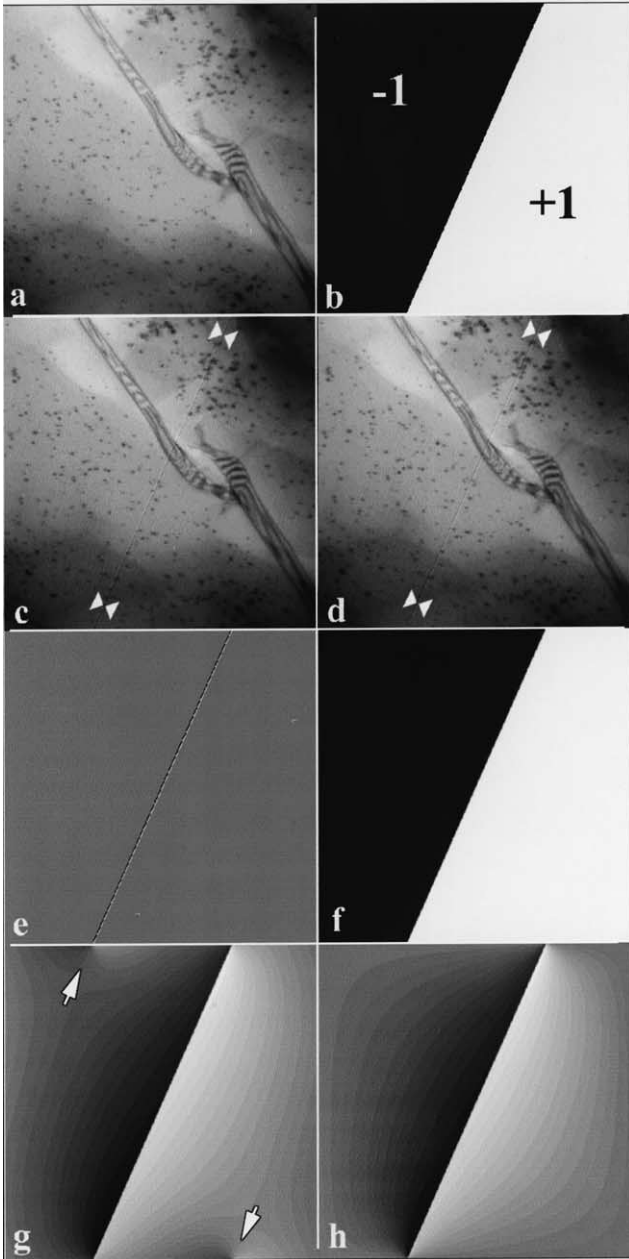


Fig. 2. Simulated phase reconstruction based on a randomly selected amplitude image (a) and a two-level phase function (b); under-focus (c) and over-focus (d) images were computed according to Eq. (16); image (e) represents the derivative $\partial I/\partial z$. The reconstructed phases are shown in (f) for the even symmetrization, (g) for a standard reconstruction without symmetrization, and (h) for the odd symmetrization.

Fig. 1(c); for the odd extension $I \cdot \partial_n \phi$ is even (Fig. 1(d)). Other possible image extensions are inconsistent with the translational periodicity required by the Fourier series approximation.

Both symmetrized image extensions satisfy all boundary conditions and the internal symmetry of the TIE equation. They are also periodic extensions so that the FFT formalism can be applied without introducing edge effects. For the even extension the function $I \cdot \partial_n \phi$ smoothly crosses zero at

the edge L , as shown in Fig. 1(c). However, the odd extension has singular zero points all along the edge (Fig. 1(d)) at the limit $\delta \rightarrow 0$; the result of this singular point is that edge effects may continue to persist in the reconstructed phase, similar to the edge effects due to non-periodic images. For this reason the even symmetric extension (Fig. 1(a)), which does not suffer from this artifact, is preferred.

3. Experimental

To demonstrate the new TIE solution method we use two images for the amplitude $A(\mathbf{r}_\perp)$ and phase $\phi(\mathbf{r}_\perp)$: a bright field image (A^2) of crack bridging in LaAlO_3 thin foil (Fig. 2(a)), and simple phase function (ϕ) equal to -1 or $+1$ radians, with a linear step boundary (Fig. 2(b)). Out-of-focus images for the wave function $\Psi = A \exp(i\phi)$ created from these two images can be computed using the following expression (De Graef, 2001):

$$I(\mathbf{r}_\perp, \Delta f) = A^2 - \frac{\lambda \Delta f}{2\pi} \nabla_\perp \cdot (A^2 \nabla_\perp \phi) \quad (16)$$

where Δf is the defocus in TEM experiment. The pre-factor $\lambda \Delta f / 2\pi$ was taken equal to 0.01. The under-focus and over-focus images computed from this relation are shown in Fig. 2(c) and (d). The images provide only amplitude information about the complex object; the linear feature associated with the phase discontinuity is just barely visible in the computed images. The image in Fig. 2(e) was calculated from their difference, and approximates the right-hand term $\partial I/\partial z$ of the TIE (2). The phase associated with the amplitude information available in the images (Fig. 2(c) and (d)) was recovered using three different methods: (1) the even symmetrized extension (Fig. 2(f)); (2) direct FFT computation without symmetrization (Fig. 2(g)); (3) the odd symmetrized extension (Fig. 2(h)).

The even symmetrized extension provides the best phase reconstruction with no detectable edge effects. The difference between the reconstructed phase ϕ' and the input phase ϕ can be described in terms of the parameter $\chi^2 = (\phi' - \phi)^2 / N^2$, where the summation covers all pixels of the $N \times N$ ($N = 512$) image. For the even symmetrization, we have $\chi^2 = 1.9 \times 10^{-3}$. For the odd symmetrization we have $\chi^2 = 4.7 \times 10^{-1}$, while for the direct FFT reconstruction without periodic continuation we have $\chi^2 = 4.3 \times 10^{-1}$. The direct FFT method suffers from edge effects (arrowed in Fig. 2(g)) and cannot reproduce the flatness of phase difference across the step-like phase boundary (Fig. 2(b)). The odd reconstruction (Fig. 2(h)) seems suffering from similar problem, but not introducing edge effects inherent to direct FFT method. The even symmetrized phase ϕ' (Fig. 2(f)) does not suffer from edge effects and is nearly identical to the input phase ϕ . The reconstructed profile across the 2-radian step in the phase map is about nine pixels wide, as opposed to the input profile that was only one pixel wide.

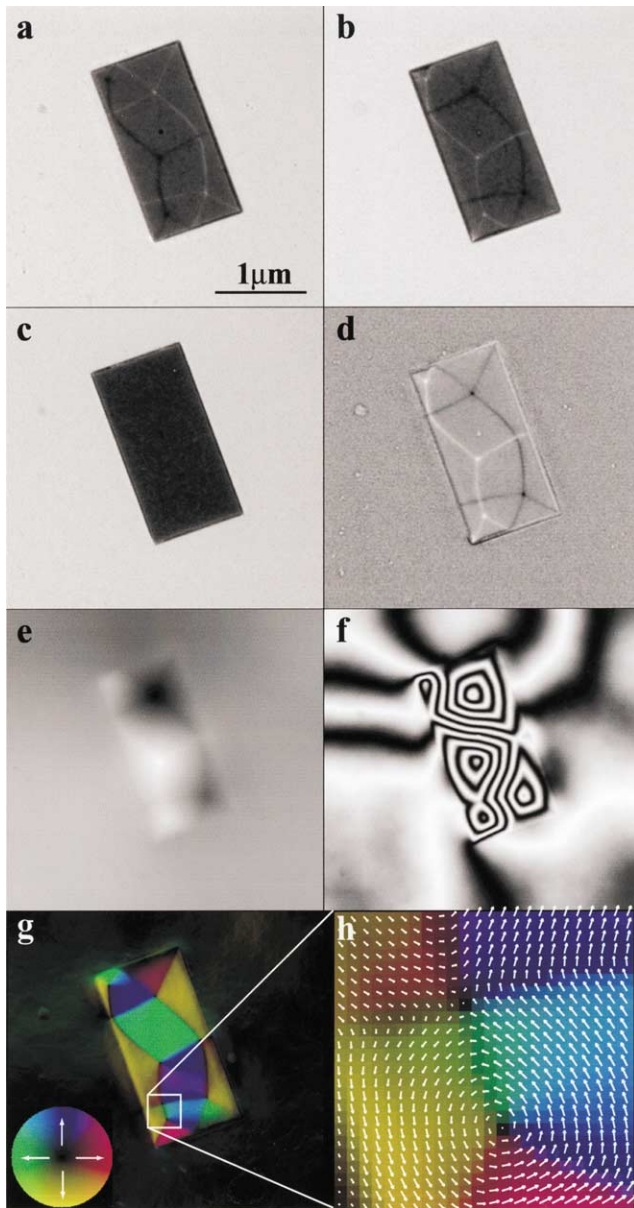


Fig. 3. Experimental phase reconstruction for a rectangular Permalloy island supported on a membrane. The under- (a), over- (b), and in-focus (c) images were obtained in a JEOL 4000EX microscope. The difference between (b) and (a) is shown in (d), and the reconstructed phase (using the even symmetrization method) in image (e). The function $\cos(10\phi)$ is shown in image (f). The local orientation of the magnetic induction (proportional to the gradient of the phase) is shown as a color plot in (g); image (h) is a magnified image of small-boxed region in (g) with the local magnetization vectors superimposed on the colored pixels. The small inset in (g) is a color wheel encoding the direction and amplitude of local magnetization in the color map.

This blurring of sharp phase edges is due to the $1/q^2$ low-pass filter character of the inverse gradient operator ∇_{\perp}^{-2} .

Fig. 3 shows a practical application of the symmetrized TIE method to an experimental data set obtained in JEOL 4000EX transmission electron microscope operated at 400 kV. The sample consists of patterned island of Permalloy on support membrane. The island shown in Fig. 3

measures $2 \times 1 \mu\text{m}^2$. The under-focus, over-focus, and in-focus images are shown in Fig. 3(a)–(c), respectively, along with the difference image between (a) and (b), which approximates $\partial I/\partial z$ in Fig. 3(d). The reconstructed phase, using the even symmetrization method, is shown in Fig. 3(e), along with $\cos(10\phi)$ in Fig. 3(f) to emphasize the spatial variations in the phase. Note that phase image (Fig. 3(e)) in fact provides more detail information about the object than the simple difference image (Fig. 3(d)) just because the image (d) in first approximation is only a Laplacian ($\nabla_{\perp}^2 \phi$) of image (e). The practical use of recovered phase map (e) and, hence a phase gradient ($\nabla_{\perp} \phi$) map become clear, especially in application to the problem of induction mapping $\mathbf{B}(x, y)$ of magnetic materials. Indeed, the phase gradient is related to the in-plane components of the integrated magnetic induction \mathbf{B} (Aharonov and Bohm, 1959) and is shown as color plot in Fig. 3(g); the color wheel indicates the correspondence between color and magnetization direction. Fig. 3(h) shows vector plot of the magnetization pattern for boxed area in Fig. 3(g) (white square) which contains both vortex and cross-tie domain wall. Correct induction mapping at nanoscale is important for general understanding of remagnetization process.

4. Conclusion

We have demonstrated that the TIE-FFT method can be used to retrieve phase information and, in particular, to map the local induction distribution (Fig. 3(g)) in magnetic materials. In comparison with the off-axis electron holography it is less technically demanding method not requiring a bi-prism. The second advantage of our approach apart from its evident simplicity is that the phase surface recovered by TIE-FFT solution is a smooth and unique ‘scalar’ function (up to a constant in the absence of intensity zeros) in accordance with Eq. (3), whose value may vary multiples of π over the entire object area, as expected from the well-known Aharonov and Bohm (1959) phase relation to electromagnetic potentials. For comparison, the phase information in electron holography is usually recovered as inverse of trigonometric function $\tan(\phi) = x/y$ with a smooth solution as $\phi = \arctan(x/y)$ that exists only on $(-\pi/2, \pi/2)$ interval, and hence total phase reconstruction has to go through the tedious and sometimes ambiguous phase-unwrapping procedure.

In summary, we have proposed new symmetrized solution method for solving the TIE using FFT. The method is fast, reliable and insensitive to noise. It provides an exact phase solution for periodic objects and a good approximation for aperiodic objects. We have also described a wide range of experimental images with non-uniform illumination of objects, for which the intensity variations recorded at the image circumference can be negligibly small, i.e. $\partial I(L)/\partial z \approx 0$. For this class of images, the symmetrization

rule will also provide a unique apart from a constant term TIE-FFT phase solution.

Acknowledgements

This research was supported by the US Department of Energy, Division of Materials Sciences, Office of Basic Energy Science, under the Contract Nos. DE-AC02-98CH10886 and DE-FG02-01ER45893 and US National Science Foundation, Division of Materials Research, Grant No. DMR-0095586. The authors would like to thank D. Paganin for his comments on draft version of this paper, M. Schofield for stimulating discussion and J. Chapman for providing the sample for Fig. 3.

References

- Aharonov, Y., Bohm, D., 1959. Significance of electromagnetic potentials in quantum theory. *Phys. Rev.* 115, 485–491.
- De Graef, M., 2001. Chapter 2: Lorentz microscopy: theoretical basis and image simulations. In: De Graef, M., Zhu, Y. (Eds.). *Magnetic Imaging and its Applications to Materials. Experimental Methods in the Physical Sciences*, vol. 36. Academic Press, New York, pp. 27–67.
- Gabor, D., 1948. A new microscopic principle. *Nature (London)* 161, 777–778.
- Gureyev, T.E., Nugent, K.A., 1996. Phase retrieval with the transport-of-intensity equation. II. Orthogonal series solution for nonuniform illumination. *J. Opt. Soc. Am. A* 13, 1670–1682.
- Paganin, D., Nugent, K.A., 1998. Noninterferometric phase imaging with partially coherent light. *Phys. Rev. Lett.* 80, 2586–2589.
- Piskunov, N., 1965. *Differential and Integral Calculus*. Noordhoff, Gronigen p. 706.
- Roddier, F., 1990. Wavefront sensing and the irradiance transport equation. *Appl. Opt.* 29, 1402–1403.
- Sneddon, I.N., 1957. *Elements of Partial Differential Equations*. McGraw-Hill, New York p. 154.
- Teague, M.R., 1982. Irradiance moments: their propagation and use for unique retrieval of phase. *J. Opt. Soc. Am.* 72, 1199–1209.
- Teague, M.R., 1983. Deterministic phase retrieval: a Green's function solution. *J. Opt. Soc. Am.* 73, 1434–1441.